JZUS

Consolidation behavior of Tianjin dredged clay using two air-booster vacuum preloading methods[*]

Hua-yang LEI[1,2,3], Yao HU[1], Jing-jin LIU[†‡1,2], Xu LIU[1], Chen-yuan LI[1]

[1]Department of Civil Engineering, Tianjin University, Tianjin 300350, China

[2]Key Laboratory of Coast Civil Structure Safety of Ministry of Education, Tianjin University, Tianjin 300350, China

[3]Key Laboratory of Earthquake Engineering Simulation and Seismic Resilience of China Earthquake Administration,

Tianjin University, Tianjin 300350, China

[†]E-mail: liujingjinljj@163.com

Abstract: This paper presents model tests (macro aspect) and microstructure tests (micro aspect) for investigating the consolidation behavior of Tianjin dredged clay using the prefabricated vertical drain air-booster vacuum preloading (PAVP) and tube air-booster vacuum preloading (TAVP) methods. The mechanism of air-booster vacuum preloading (AVP) using a spring-like system is explained. The main difference between these two methods is the air-boosting equipment. A new anticlogging air-booster prefabricated vertical drain (PVD) is used in the PAVP technique and a self-designed air-booster tube is used in the TAVP technique. In the model tests, a comparison of the variables that are monitored during reinforcement (vacuum pressure, surface settlement, water discharge, and pore-water pressure) and after reinforcement (water content, dry density, and vane shear strength) is conducted. The results indicate that the consolidation behavior of Tianjin dredged clay using the PAVP method is better than that using the TAVP method. PAVP more efficiently mitigates the issue of water-draining PVD clogging and significantly accelerates drainage consolidation. In addition, in the microstructure tests, a comparison of the variables that are monitored after reinforcement (via scanning electron microscopy (SEM) and mercury intrusion porosimetry (MIP)) is conducted, and the results further explain the model test results.

Key words: Tianjin dredged clay; Prefabricated vertical drain air-booster vacuum preloading (PAVP); Tube air-booster vacuum preloading (TAVP); Model test; Microstructure test

https://doi.org/10.1631/jzus.A2000133   **CLC number:** TU447

1 Introduction

Land reclamation is an effective approach for alleviating the shortage of land resources. As of 2019, the total land area for reclamation in China has exceeded 1100 km^2 and is growing by 13% annually.

Tianjin is located in the Bohai Bay, and has completed 320 km^2 of land reclamation. As a typical example, the Tianjin Lingang Economic Zone, with a reclamation area of 200 km^2, is located in the shallow sea area on the south side of the Haihe estuary (shown in Fig. 1) and is formed largely of dredged clay.

Dredged clay is formed by hydraulic filling using slurry from a harbor basin or a sea channel (Li et al., 2009; Ong and Chai, 2011; Lei et al., 2017b; Liu et al., 2018; Wang et al., 2018, 2019), and is typical of ultra-soft soils. It possesses poor physical and mechanical properties, such as a high-water content, high void ratio, high compressibility, low permeability, and low bearing capacity (Chu and Yan, 2015;

Liu et al., 2017; Zheng et al., 2017; Wang et al., 2019). Therefore, there are many serious problems of engineering geology to be solved by ground improvement techniques before a project can go forward.

Fig. 1 Tianjin Lingang Economic Zone with land reclamation, China (Amap, annotations made by the authors)

Vacuum preloading methods have been widely used in solving these problems of engineering geology (Bergado et al., 2002; Yan and Chu, 2005; Chai et al., 2006; Indraratna et al., 2014; Cai et al., 2017). However, this kind of ultra-soft soil is not suitable for traditional vacuum preloading methods. Until now, studies have made some progress, but there are still some uncertainties concerning vacuum preloading in soft soil consolidation, particularly in handling the dredged clay with its ultrahigh moisture content, for example, the clogging of prefabricated vertical drains (PVDs) (Chu and Yan, 2015; Lei et al., 2017a) and the loss of vacuum pressure (Chai et al., 2004). The clogging of water-draining PVDs is one of the main factors affecting the consolidation behavior of dredged clay using vacuum preloading. How to eliminate the water-draining PVD clogged layer and realize a rapid consolidation are key problems that need to be resolved urgently.

To address this problem, a new type of air-booster vacuum preloading (AVP) method for dredged clay has been suggested (Shen et al., 2015; Wang et al., 2016; Lei et al., 2017a, 2020; Cai et al., 2018). The basic principle of AVP consists of the following three steps: (1) when the air-booster pressure is applied, the pressure difference between the air-booster PVD/tube and water-draining PVD squeezes the soil and stimulates the flow of water; (2) the water flow can exit the water-draining PVD and carry off the fine soil particles of the clogging; (3) the airflow can create additional cracks under the pressure difference, and can shorten the leakage path and accelerate drainage consolidation of the soil (Azari et al., 2016; Lei et al., 2017a, 2020). At present, there are two main air-booster methods: (1) the PVD AVP (PAVP) method, which involves the direct use of PVDs for air-boosting purposes (Cai et al., 2018), and (2) the tube AVP (TAVP) method, which uses a self-developed booster tube for air-boosting purposes (Lei et al., 2020). Current research on the consolidation behavior of dredged clay using the AVP method has achieved some progress, but there are few studies on the differences between these two AVP methods and it is necessary to compare the consolidation behaviors of dredged clay when using them.

In this paper, the consolidation behavior of Tianjin dredged clay using the PAVP (which uses a new anti-clogging air-booster PVD) and TAVP (which uses a self-developed air-booster tube) methods are investigated by model tests and microstructure tests. Firstly, we explain the mechanism of the AVP method using a spring-like system and the main differences between the two methods. Secondly, the difference of consolidation behaviors for Tianjin dredged clay between the PAVP and TAVP methods is discussed from a macro aspect (model tests) and a micro aspect (microstructure tests). Based on the results and analyses of these two tests, a superior AVP method for treating that clay will be proposed.

2 PAVP and TAVP

2.1 Mechanism of the AVP method

Fig. 2a shows the overall system of the AVP method. It consists of a vacuum pump, a water-air separation equipment, a horizontal drain tube, a horizontal air-booster tube, a pressed film groove, an air-booster equipment (PVD/tube), water-draining PVDs, and an air compressor. According to Cai et al. (2018) and Lei et al. (2020), the system can generate pressure differences between the water-draining PVDs and the air-booster equipment (PVD/tube) and more fissures will also be generated, thereby alleviating water-draining and PVD clogging, and improving the consolidation behavior of the dredged clay.

In addition, the process of formation is as follows: in the air-boosting stage, the discontinuous pores in the soil are filled with air, forming a certain

air pressure to squeeze the soil. When the pressure is greater than the critical strength of the soil, discontinuous pores will be connected, and the soil will perform an irregular fracture expansion, thereby forming fissures in the soil (Katsman et al., 2013; Ye, 2018). In the non-air-boosting stage, these fissures will become drainage channels and improve the consolidation behavior of the clay.

(a)

(b)

Fig. 2 Air-booster vacuum preloading: (a) system and (b) mechanism (courtesy of Lei et al. (2020))
p_a: atmospheric pressure; u_0: initial pore-water pressure; Δu: variation in the pore-water pressure caused by vacuum pressure; $\Delta u'$: variation in the pore-water pressure caused by the air-booster; $\Delta\sigma$: incremental effective stress

Fig. 2b explains the mechanism of the AVP method using a spring-like system (Lei et al., 2020). Initially, the atmospheric pressure p_a acts on the system and produces an equal initial pore-water pressure u_0 ($u_0=p_a$). Then, vacuum pressure is imposed on the system to create a negative variable pore-water pressure $-\Delta u$. Finally, air-booster pressure is applied to the system to generate a negative variable pore-water pressure $-\Delta u'$. Therefore, the total pore-water pressure is the sum of the variation in pore-water pressure caused by vacuum pressure Δu and the variation in pore-water pressure caused by the air-booster

$\Delta u'$. Based on the effective stress theory, the total stress is kept constant (i.e. atmospheric pressure p_a), and the increase in effective stress is equal to the decrease in pore-water pressure. Hence, the incremental effective stress $\Delta\sigma$ is the sum of Δu and $\Delta u'$, i.e. $\Delta\sigma=p_a-(u_0-\Delta u-\Delta u')=\Delta u+\Delta u'$, and the soil skeleton is compressed by $\Delta\sigma$.

2.2 Difference between the PAVP and TAVP

The main difference between the PAVP and TAVP methods is the air-booster equipment. The new anticlogging air-booster PVD, which is used in the PAVP method, is shown in Fig. 3a. The air-booster PVD is composed of a core plate (made from polypropylene) and a filter sleeve (made from nonwoven polypropylene geotextile), which are glued together. The core is used to retain the shape of the PVD in the soil, and the filter sleeve is applied to ensure water drainage from the soil through the PVD. Compared with the traditional air-booster PVD (Fig. 3c), its core plate and filter sleeve are separated, which increases the transfer path and thus the new air-booster PVD can improve the vacuum transmission capacity, increase the strength of the PVD, and prevent the filter from becoming damaged. In addition, the aperture of the air-booster PVD can be adjusted according to the test effect, the water permeability is greatly improved, and clogging is effectively prevented.
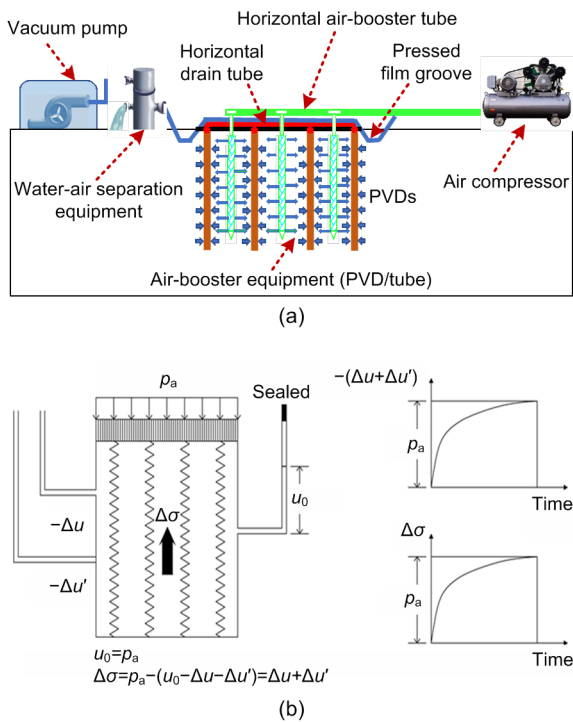

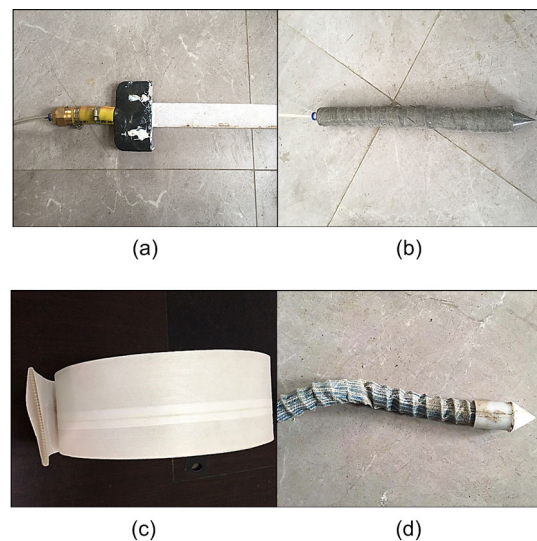(a)   (b)

(c)   (d)

Fig. 3 Air-booster equipment (PVD/tube): (a) new air-booster PVD; (b) new air-booster tube; (c) traditional air-booster PVD; (d) traditional air-booster tube

Fig. 3b presents the self-designed air-booster tube under the TAVP method. The booster tube is composed of a skeleton (made from iron) and a mesh (made from wire). The role of the skeleton is to retain the shape of the tube in the soil, and the role of the mesh is to guarantee that the compressed gas is injected into the soil from the sides of the tube. Compared with traditional booster tubes (Fig. 3d) that contain spiral flexible brackets and filter cloths, which have a low stiffness and air permeability, the self-designed tube has a higher stiffness and air permeability, which is convenient for intubation and increased air-booster effects.

3 Methodology

3.1 Soil sample

In this study, a type of dredged clay that is widely distributed within dredged clay from the Tianjin Lingang Economic Zone was used. Table 1 shows the basic physical indices of the soil, among which are a water content of 117.5% and a plasticity index of 34.65.

Table 1 Basic physical indexes of the remolded soil samples

Index property	Value
Specific gravity, G_s	2.7
Initial water content, w (%)	117.5
Initial void ratio, e_0	3.98
Liquid limit, w_L (%)	63.87
Plastic limit, w_P (%)	29.22
Plasticity index, I_P (%)	34.65
Wet density, ρ (g/cm³)	1.18

3.2 Model test

3.2.1 Test apparatus

Fig. 4a introduces the experimental set-up of the AVP model test. It consisted of an air compressor, a model test chamber (water-draining PVDs, an air-booster PVD/tube, a horizontal drain tube, a sealing membrane, and a geotextile were arranged inside), a water-air separation tank, and a vacuum pump. The model test chamber was made of plexiglass plate, and had internal dimensions of 80 cm×60 cm×70 cm.

The four water-draining PVDs were arranged in a square shape, and an air-booster PVD/tube was installed in the center (Fig. 4b). To minimize the boundary effect, all the PVDs were transformed before the AVP model test. According to the dimensions of the model test chamber, the width of the water-draining PVDs, the distance between the water-draining PVDs, and the length were calculated by Eqs. (1) and (2) as 3 cm, 30 cm, and 45 cm, respectively. In addition, the locations of the measuring points for the model tests before and after reinforcement are presented in Figs. 5a and 5b, respectively. The specific calculation equation is as follows (Lei et al., 2020):

$$d_w = \frac{b+t}{2}, \tag{1}$$

where d_w, b, and t are the equivalent drain diameter, width, and thickness of the band-shaped water-draining PVD, respectively.
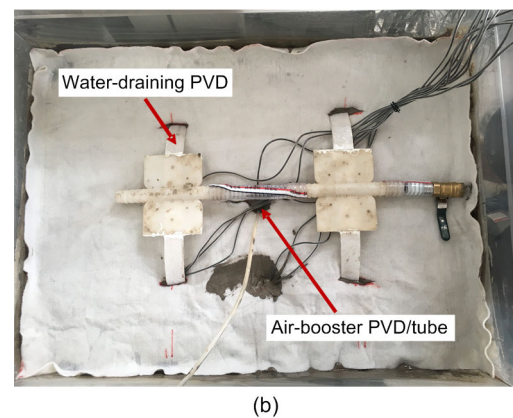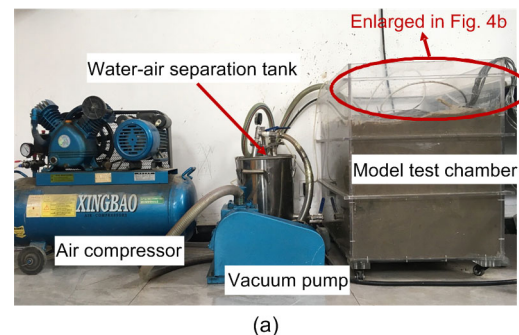

(a)

(b)

Fig. 4 Air-booster vacuum preloading model test: (a) experimental set-up, (b) layout of water-draining PVDs and air-booster PVD/tube

$$n = \frac{d_e}{d_w}, \qquad (2)$$

where ratio n=15–22 (Cai et al., 2018); d_e is the effective diameter of influence (Lei et al., 2020).

○ Pore pressure (P); ● Vane shear strength (V); □ Settlement (S); ■ Dry density (D); ▲ Water content (W); × SEM (S); □ MIP (M)
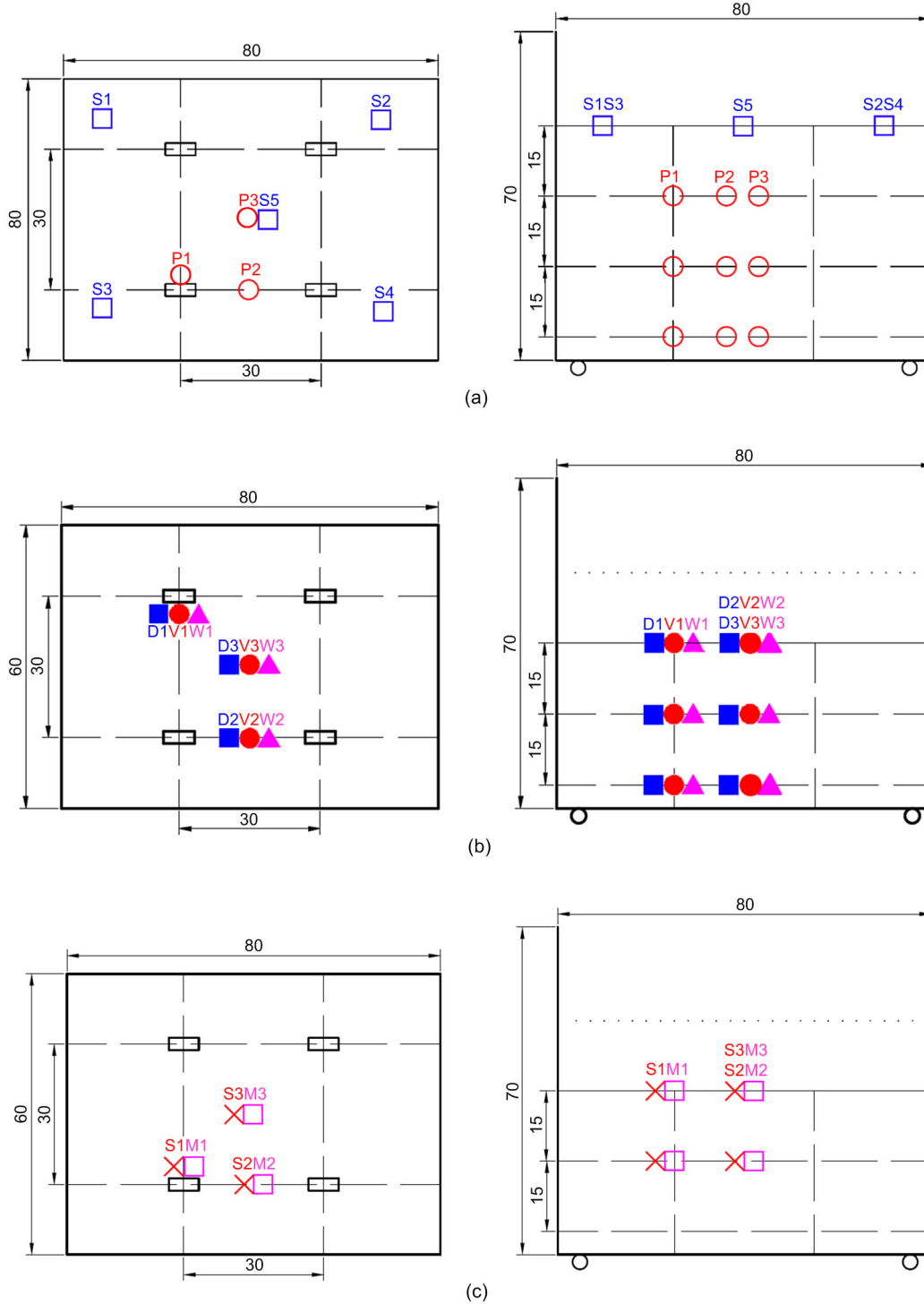
Fig. 5 Locations of the measuring points for the model tests before (a) and after (b) reinforcement, and for the microstructure test (c) (left is top view and right is front view) (unit: cm)

3.2.2 Test procedure and scheme

In this study, two sets of model tests (PAVP and TAVP) are compared to assess the consolidation behavior of Tianjin dredged clay and are summarized in Table 2. The precise procedures of the test plan were as follows: (1) The vacuum pressure was 80 kPa, and the air-booster pressure was 150 kPa (Lei et al., 2020); the air-booster pressure was activated every 24 h by opening the air compressor, and the air compressor was operated for 45, 60, and 90 min at the times of 188, 284, and 380 h, respectively. (2) When the surface settlement was less than 2 mm/d, the water output was smaller than 0.2 kg/d, and the pore-water pressure dissipation was lower than 0.02 kPa/d for three consecutive days, the test was stopped. (3) During the test, the vacuum pressure, surface settlement, water discharge, and pore-water pressure were monitored, and the water content, dry density, and shear strength were measured after the test.

3.3 Microstructure test

3.3.1 Test scheme

The microstructure of a soil largely determines its engineering properties, and the changes in microstructure are fundamental to its strength and deformation characteristics (Inyang et al., 2007; Yu et al., 2019). In this study, a microstructure test was conducted in combination with scanning electron microscopy (SEM) and mercury intrusion porosimetry (MIP) to give an improved analysis of the microstructure of soil. Furthermore, after the PAVP and TAVP reinforcements, microstructure tests (SEM and MIP) of the dredged clay were performed at various locations (S1, S2, S3, M1, M2, and M3) and depths (0 and 15 cm); the locations of the measuring points for the microstructure tests are shown in Fig. 5c. Among them, the soil microscopic unit characterization with respect to its geometry, arrangement, connection, and most of the microscopic parameters (such as the

porosity, shape factor, and fractal dimension) were primarily obtained by the SEM tests, while the MIP tests determined the pore diameter distribution of the soil more accurately.

3.3.2 Quantitative analysis of the microstructure parameters via SEM

Image-Pro Plus image processing software was used to binarize the SEM images, and certain parameters were extracted for the quantitative analysis of microstructures. The meaning and algorithm of the microstructure parameters are briefly described as follows (Hyslip and Vallejo, 1997; Arasan et al., 2011):

(1) Porosity: The porosity is the percentage of the pores in the soil to the total volume of the soil, that is, the ratio of the pore volume in the soil to the total volume of the soil.

(2) Fractal dimension:

$$L(\varepsilon) = L_0 \varepsilon^{1-D}, \qquad (3)$$

where D is the fractal dimension of the pores, L_0 is a constant, ε is the length of pore curve, and $L(\varepsilon)$ is the fractal curve. D depicts the degree of roughness of the curve, that is, the degree of roughness of the shape of the pore curve.

4 Results and discussion

4.1 Model test

4.1.1 Vacuum pressure

The pressure gauge installed on the water-air separation tank was used to directly capture the vacuum pressure in time. The variation curves of the vacuum pressure of the PAVP and TAVP tests for the overall process are shown in Fig. 6a. In the two model tests, the influence of the air-booster on vacuum pressure could be divided into two phases. In the first

Table 2 Model test schemes for PAVP and TAVP

Test	Vacuum pressure (kPa)	Booster pressure (kPa)	Booster activation time (h)	Duration of boosting (min)	Measured variable (during test)	Measured variable (after test)
PAVP/ TAVP	80	150	188, 284, 380	45, 60, 90	Vacuum pressure, surface settlement, water discharge	Water content, dry density, vane shear strength

phase, the variation trends of the vacuum pressure with time were similar; the vacuum pressure remained almost stable and exhibited very slight fluctuations at approximately 80 kPa before air-boosting (before 188 h). In the second phase, the curve of the vacuum pressure for the PAVP test was higher than that of the TAVP test, but declined gradually during the air-boosting processes (at 188 h, 284 h, and 380 h) and eventually reached approximately 72 kPa in the PAVP test and 70 kPa in the TAVP test. These results demonstrated that the PAVP method has a better effect on the variations in surface vacuum pressure.

Fig. 6 Variation curves of the vacuum pressure in time during the PAVP and TAVP tests: (a) overall process; (b) first air-boosting process at 188 h

Fig. 6b displays the variation curves of the vacuum pressure with time for the PAVP and TAVP tests during the first air-boosting process at 188 h. The vacuum pressure of the PAVP test was always higher than that of the TAVP test after the first air-boosting process at 188 h. The variation in vacuum pressure due to the first air-boosting process could be split into

three stages: rapid decline, stable behavior, and sharp rise. When the air-booster was activated, the vacuum pressure in the two tests rapidly declined at approximately the same rate. The vacuum pressure due to the first air-boosting process then remained relatively stable. When the air-booster was stopped, the vacuum pressure in the two tests rose sharply at approximately the same rate.

4.1.2 Water discharge

Fig. 7a reveals the variation curves of the water discharge with time of the PAVP and TAVP tests during the overall process. The water discharge was collected in a water-air separation tank and weighed by the electronic scale underneath the tank. The overall trend of the two curves of the two tests was similar. The trend could be divided into three stages: a rapid growth stage, a slow growth to stability stage, and another growth stage. In the first stage (from 0 to 68 h), when the vacuum pump was started, the curves of the water discharge for the two methods rapidly increased at almost the same rate. In the second stage (from 68 to 188 h), the curves slowly grew and then remained relatively stable. In the third stage (after 188 h), when the air-booster was activated (at 188 h), growth curves occurred again and a maximum value was achieved. The values of the water discharge for the PAVP and TAVP tests were 48.51 kg and 42.61 kg, respectively, and thus the final discharge of the PAVP method was higher than that of the TAVP by more than 13.85%. The water discharge is a very important indicator for evaluating the effect of vacuum preloading, which is proportional to the processing effect (Lei et al., 2017a). This finding showed that, for dredged clay, the effect of the PAVP method was greater than that of the TAVP method.

To further evaluate the influence of air-boosting, the PAVP test is selected as an example. It can easily be seen that the curve after 188 h (during the air-boosting process) exhibits the following features: three increases occurred at 188 h (air-boosting for 45 min), 284 h (air-boosting for 60 min), and 380 h (air-boosting for 90 min), and the upward trend decreased accordingly. The latter was because that the time periods of the three air-boosting processes were different.

Fig. 7b shows the variation curves of the water discharge with time of the PAVP and TAVP tests
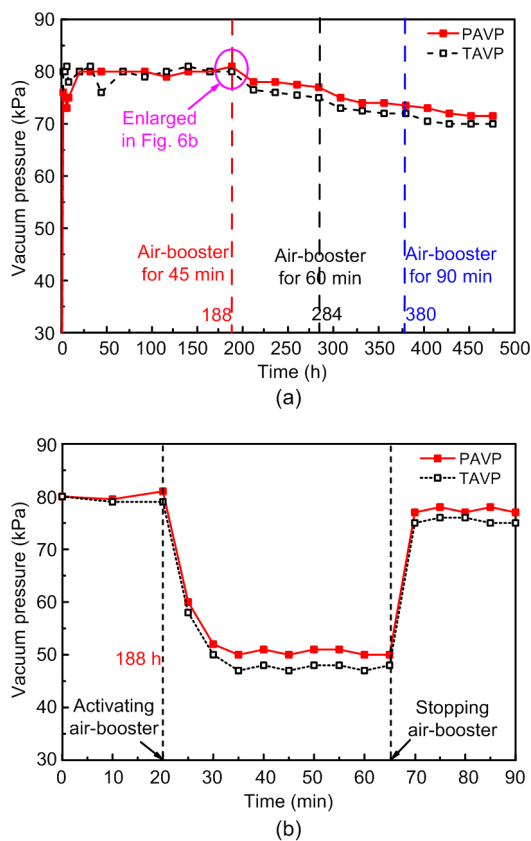
during the first air-boosting process at 188 h. The level of water discharge in the PAVP test was definitely higher than that of the TAVP test. This result shows that the PAVP method has an improved effect on the water discharge. In addition, both curves showed a similar trend, and rapidly rose in the first 10 min, after which the growth rate slowed down and finally stabilized. These results indicated that the air-boosting process has its most significant effect towards the beginning of its operation (from 20 min to 30 min in Fig. 7b).
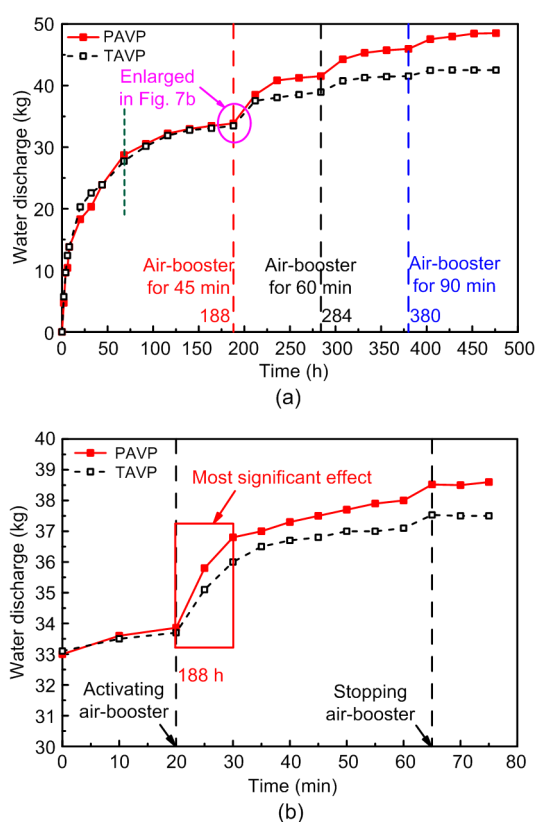

Fig. 7 Variation curves of the water discharge with time of the PAVP and TAVP tests: (a) overall process; (b) first air-boosting process at 188 h

4.1.3 Surface settlement

Fig. 8 shows the variation curves of the surface settlement with time of the PAVP and TAVP tests, which were obtained by calculating the average of five monitoring points (Fig. 5a). The curves of surface settlement during the whole vacuum preloading period could be split into two parts. First, before the air-booster was activated, the surface settlements under

the two situations virtually corresponded, and gradually increased until remaining stable at 188 h. After the air-booster was activated, the surface settlement in the PAVP test was greater than that in the TAVP test. The settlements eventually reached the maxima of 15.40 cm and 13.40 cm, respectively. The surface settlement in the PAVP test had increased by 14.93% compared with that in the TAVP test. Generally, therefore, the PAVP method is considered effective for the AVP treatment of Tianjin dredged clay. In addition, when the air-booster was activated, surface settlement occurred three times as sudden increases at 188 h (air-boosting for 45 min), at 284 h (air-boosting for 60 min), and at 380 h (air-boosting for 90 min). The sudden increases were because the time intervals of the three air-boosting processes were different. In other words, the air-boosting effect improved with increasing duration of the process.
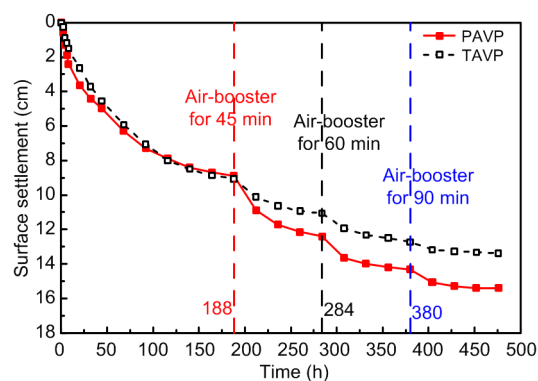

Fig. 8 Variation curves of the surface settlement with time of the PAVP and TAVP tests

4.1.4 Coefficient of consolidation

The coefficient of consolidation (C_v) is a parameter that reflects the degree of consolidation of soft soil. To better investigate these consolidation characteristics, C_v was determined and analyzed. C_v was back-calculated by Liu et al. (2017) as follows:

$$C_v = -\frac{H^2 \ln \beta_1}{6 \Delta t}, \quad (4)$$

$$S_i = \beta_0 + \beta_1 S_{i-1}, \quad (5)$$

where H is the length of the water-draining PVDs, β_0 is a constant, β_1 is a coefficient which is obtained by

the Asaoka method, and Δt is the time interval. The settlement curve between settlements S_i and S_{i-1} (Fig. 9) was used to define Eq. (5) and obtain β_1 in Eq. (4). As shown in Fig. 9, the values of β_1 were 0.8574 and 0.8883 for the PAVP and TAVP tests, respectively. In addition, the length H of the water-draining PVDs was 45 cm, and the time interval Δt was 24 h.

Table 3 lists the coefficients of consolidation and parameters of the PAVP and TAVP tests. According to the values of all parameters (H, β_1, and Δt), the coefficients of consolidation (C_v) could be calculated by substituting the values into Eq. (4). That yielded values of 0.000 601 cm²/s and 0.000 463 cm²/s for the PAVP and TAVP tests, respectively. It was observed that the compression performance and stimulation of soil consolidation had improved and the outcomes were consistent with the aforementioned analyses.

Table 3 Coefficients of consolidation and parameters of the PAVP and TAVP tests

Test	H (cm)	Δt (h)	β_1	C_v (cm²/s)
PAVP	45	24	0.8574	0.000 601
TAVP	45	24	0.8883	0.000 463

4.1.5 Pore-water pressure

Fig. 10 shows the variation curves of the pore-water pressure with time of the PAVP and TAVP tests at different positions (at depths of 15 cm, 30 cm, and 45 cm and at measuring points P1, P2, and P3, respectively). It should be noted that the "fault" in the figure reflects a data acquisition error. Overall, the pore-water pressure decreased in time at the various depths and measuring points. The variation in pore-water pressure could be divided into four phases: rapid reduction, slow decrease, leveling off, and again reduction.

Taking Fig. 10b as an example, in the first phase (from 0 to 44 h), in the PAVP and TAVP tests, the pore-water pressure dropped rapidly after the start of the tests. In the second phase (from 44 to 140 h), the pore-water pressure slowly decreased. In the third phase (from 140 to 188 h), the pore-water pressure dissipation tended to level off. In the fourth phase (after 188 h), the pore-water pressure again exhibited three reductions at 188 h, 284 h, and 380 h, which were due to the quickening of pore-water pressure dissipation caused by the air-booster. The maximum pore-water pressure values for the PAVP and TAVP tests were −36.18 kPa and −32.18 kPa at a depth of 15 cm, respectively. The maximum value of the PAVP test was 12.4% higher than that of the TAVP test. Furthermore, the pore-water pressure increased at depths from 15 to 45 cm in both tests. In the PAVP test, the final pore-water pressures at the shallowest depth (15 cm), intermediate depth (30 cm), and deepest depth (45 cm) were −36.18 kPa, −30.50 kPa, and −26.27 kPa, respectively; in the TAVP test, the final values were −32.18 kPa, −28.24 kPa, and −23.18 kPa from the shallowest depth (15 cm) to the deepest depth (45 cm), respectively. Based on the above analysis, the results clearly indicate that the final pore-water pressure of the PAVP test is lower than that of the TAVP test, and demonstrate that the PAVP method has a more profound effect on the improvement of the dredged clay.
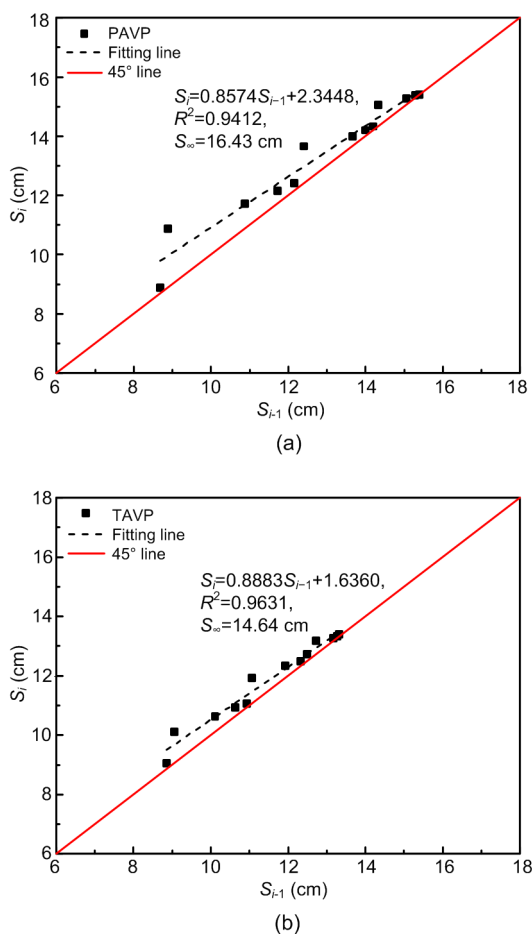

Fig. 9 Asaoka method to calculate the ultimate settlement S_∞: (a) PAVP test; (b) TAVP test

In figure (a):
$S_i = 0.8574 S_{i-1} + 2.3448$,
$R^2 = 0.9412$,
$S_\infty = 16.43$ cm

In figure (b):
$S_i = 0.8883 S_{i-1} + 1.6360$,
$R^2 = 0.9631$,
$S_\infty = 14.64$ cm
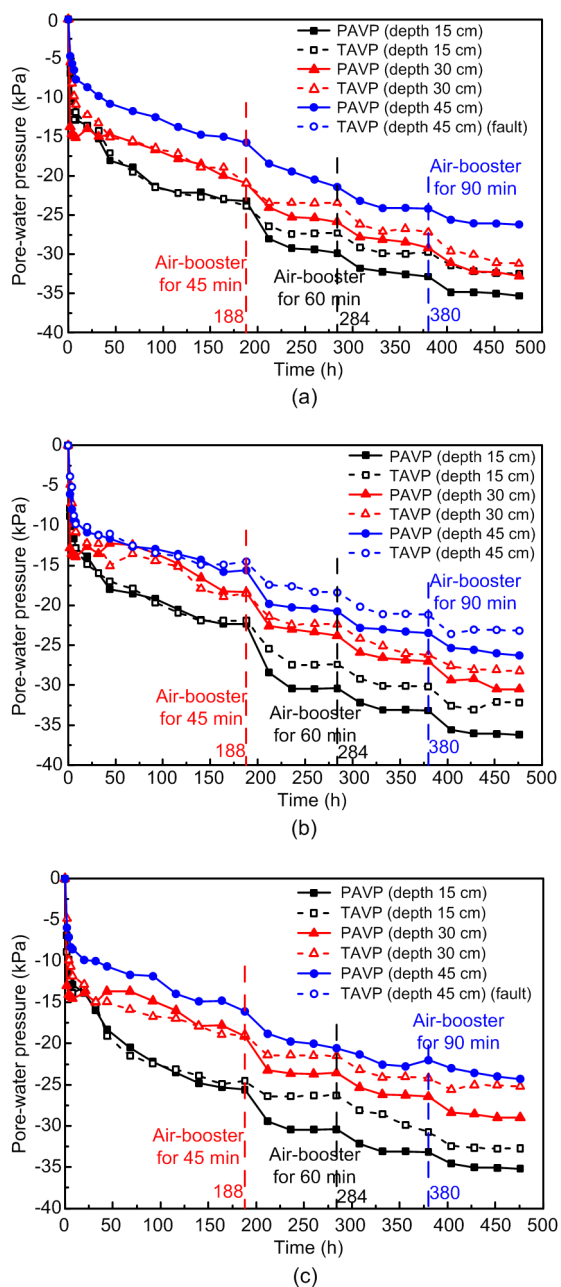
(a)

(b)

(c)

Fig. 10 Variation curves of the pore-water pressure in time of the PAVP and TAVP tests: (a) measuring point P1; (b) measuring point P2; (c) measuring point P3 (the "fault" represents a failure of data collection)

4.1.6 Water content

Water content is an important indicator for evaluating the effects of soil properties after vacuum preloading reinforcement. The water contents at different depths (0 cm, 15 cm, and 30 cm) and measuring points (W1, W2, and W3) (Fig. 5) after the PAVP and

TAVP tests are presented in Fig. 11a. At the different depths and measuring points, the water contents in the PAVP test were always smaller than those in the TAVP test. Moreover, the basic developments of the water contents were approximately parallel for both tests: the water content increased with increasing depth (from 10 to 30 cm) and measuring points (from W1 to W3). The reason for this was that the vacuum pressure dissipated as a function of the measuring point (the water-draining PVD distance increased from W1 to W3) and drainage depth (Indraratna et al., 2005; Wang et al., 2017).
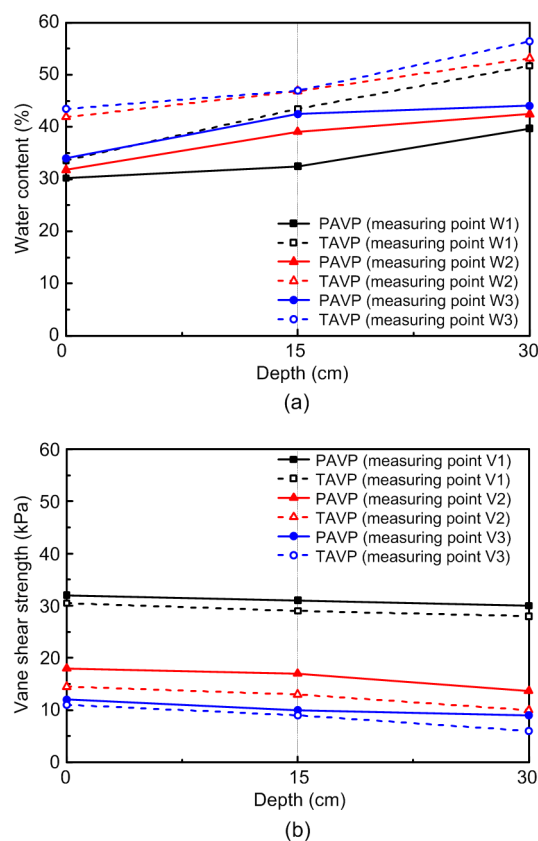

(a)

(b)

Fig. 11 After air-booster vacuum preloading reinforcement: (a) water content and (b) vane shear strength

Before treatment, the initial water content of the soil was greater than 117%. After treatment, in the PAVP test, the average water contents of the soil at the different measuring points were 31.97% (depth of 0 cm), 37.98% (depth of 15 cm), and 44.05% (depth of 30 cm), while the average water contents of the soil in the TAVP test were 39.63%, 45.77%, and 53.75%, respectively. It can therefore be seen that the PAVP

test decreases the water content compared with the TAVP one by 19.34%, 17.92%, and 18.04%, respectively, at the three different depths considered. The consolidation behavior of Tianjin dredged clay by the PAVP method is thus greater than that by the TAVP method.

4.1.7 Dry density

The dry density is often used as a criterion to evaluate soil in engineering. The dry densities at different depths (0 cm, 15 cm, and 30 cm) and measuring points (D1, D2, and D3) (Fig. 5) after the PAVP and TAVP tests are summarized in Table 4. The equation for dry density is as follows:

$$\rho_d = \frac{\rho}{1+w}, \tag{6}$$

where ρ_d is the dry density, ρ is the density of the soil after reinforcement (ρ was measured by the cutting ring method), and w is the water content of the soil before reinforcement.

As shown in Table 4, the dry density and water content of the soil after reinforcement exhibited opposite characteristics at the different depths and measuring points, but the value from the PAVP test was always higher than that from the TAVP test. Moreover, the dry density decreased with increasing depth and measuring point from W1 to W3 in the two tests. Specifically, in the PAVP test, the maximum value was 1.47 g/cm^3 at measuring point D1 and a depth of 0 cm, and the minimum value was 0.97 g/cm^3 at measuring point D3 and a depth of 30 cm. In the TAVP test, the maximum value was 1.21 g/cm^3 and the minimum value was 0.87 g/cm^3 compared with the PAVP test results at the same positions. The negative correlation between the dry density and water content is expected from Eq. (6) as they are inversely related. Based on the previous analysis, the consolidation behavior of the dredged clay using the PAVP method was enhanced compared to that from the TAVP method.

4.1.8 Vane shear strength

To assess the effects of the soil properties, the vane shear strength was measured with a manual vane shear instrument. Fig. 11b shows the vane shear strength of dredged clay at dissimilar depths (0 cm,

15 cm, and 30 cm) and measuring points (V1, V2, and V3) (Fig. 5) after the two tests. The vane shear strength value of the PAVP test was constantly higher than that of the TAVP test at different depths and measuring points. In addition, the vane shear strength decreased with increasing depth from 10 to 30 cm and measuring point from W1 to W3 for both tests. These results revealed that, because of the high vacuum pressure, a better reinforcement effect was obtained at a shallow depth and a position that was near the water-draining PVDs (Indraratna et al., 2005).

Table 4 Dry densities at different measuring points after the PAVP and TAVP tests

Depth (cm)	Dry density (g/cm^3)					
	PAVP			TAVP		
	D1	D2	D3	D1	D2	D3
0	1.47	1.25	1.17	1.21	1.08	0.99
15	1.30	1.10	1.02	1.16	1.04	0.92
30	1.20	1.07	0.97	1.14	0.97	0.87

Generally, the average vane shear strengths of the soil in the PAVP test at the different measuring points were 31.00 kPa (depth of 0 cm), 16.23 kPa (depth of 15 cm), and 10.33 kPa (depth of 30 cm), higher than those in the TAVP test, which were 29.17 kPa, 13.50 kPa, and 8.67 kPa (at depths of 0 cm, 15 cm, and 30 cm, respectively). The PAVP test clearly showed increases in vane shear strength of 6.27%, 20.22%, and 19.14%, above the respective figures from the TAVP test. The vane shear strength in the PAVP test was thus higher than that in the TAVP test at the different depths and measuring points.

According to the vane shear strength, the characteristic value of the foundation bearing capacity can be calculated. The equation is as follows (Chu et al., 2000):

$$f_a = 5.14 C_u, \tag{7}$$

where C_u is the average vane shear strength of the soil, and f_a is the characteristic value of the foundation bearing capacity. Thus, in the PAVP test, the characteristic values of the foundation bearing capacity at the different measuring points were obtained as 159.34 kPa, 83.44 kPa, and 53.11 kPa at depths of 0 cm, 15 cm, and 30 cm, respectively; in the TAVP

test, the characteristic values were 149.92 kPa (depth of 0 cm), 64.25 kPa (depth of 15 cm), and 44.55 kPa (depth of 30 cm). It can be seen that the foundation bearing capacity from the PAVP test was larger than that from the TAVP test. Combining the vane shear strengths and foundation bearing capacities, one could easily observe that the results were similar to those of the water content, and the effect of the PAVP test was superior to that of the TAVP test.

4.1.9 Degree of consolidation

The degree of consolidation (DOC) is a significant parameter or index for estimating the consolidation behavior of the clay. To further consider the effect of soil improvement, the DOC of soil was determined and analyzed. The DOC can be obtained via settlement Eqs. (8) and (9) or pore-water pressure Eqs. (10) and (11). The settlement-obtained DOC can be calculated as follows:

$$U_t = \frac{S_t}{S_\infty}, \tag{8}$$

$$S_\infty = \frac{\beta_0}{1 - \beta_1}, \tag{9}$$

where U_t is the DOC at time t, S_t is the settlement at time t, and S_∞ is the ultimate settlement. In this method, based on the Asaoka method for forecasting the ultimate settlement S_∞, the intersection of the settlement curve between S_i and S_{i-1} and the 45° line is considered the ultimate settlement S_∞ (Chu and Yan, 2015; Liu et al., 2017); S_∞ can also be calculated with Eq. (9). As an alternative, the pore-water pressure-based DOC can be calculated as follows:

$$U_{avg} = 1 - \frac{\int [u_f(z) - u_s] dz}{\int [u_0(z) - u_s] dz}, \tag{10}$$

$$u_s = \gamma_w z - 80, \tag{11}$$

where U_{avg} is the average DOC, $u_f(z)$ is the ultimate pore-water pressure at depth z, $u_0(z)$ is the initial pore-water pressure at depth z, u_s is the vacuum pressure at depth z, and γ_w is the unit weight of water.

In this study, the DOC was calculated by settlement using Eqs. (8) and (9). As shown in Fig. 9, the ultimate settlement was 16.43 cm and 14.64 cm in the PAVP and TAVP tests, respectively. The DOC at different times in the PAVP and TAVP tests are summarized in Table 5. Comparing the values in Table 5, except for 188 h, the U_t of the PAVP test was generally higher than that of the TAVP test at different times (284 h, 380 h, and at the end). The reason was that the first air-boosting process began operating at 188 h, and the settlement of the two tests was basically the same before 188 h. After 188 h, the air-booster pressure started to work and promoted settlement of the soil. Therefore, the values of the DOC in the PAVP test (which were 76%, 89%, and 94% at 284 h, 380 h, and at the end, respectively) exceeded the values of the DOC in the TAVP test (which were 75%, 86%, and 91% at 284 h, 380 h, and at the end, respectively) in time. It was clear that the consolidation effect of the PAVP method was greater than that of the TAVP method.

Table 5 Degrees of consolidation at different times

Test	DOC (%)			
	188 h	284 h	380 h	End
PAVP	54	76	89	94
TAVP	62	75	86	91

4.2 Microstructure test

4.2.1 Microstructure characteristics

In the two reinforcement modes of the PAVP and TAVP tests, the microstructure changes at the three measuring points were similar. Therefore, only measuring point S3 was selected as an example for qualitative analysis of the microstructure of the soil sample. Fig. 12 shows an SEM image that was magnified 6000 times at measuring point S3 of the clay after the PAVP and TAVP model tests. The microstructure characteristics of the soil were examined, and the analysis was in three parts: skeleton particle morphologies, skeleton particle contact forms, and intraframework grain pores. The specific analysis results were as follows:

4.2.1.1 Skeleton particle morphologies

In the two reinforcement methods, the skeleton particle morphologies of the dredged clay were primarily composed of sheet and block structures and a

few granular structures. The sheet and block structures were agglomerated, and the granules and aggregates with smaller sizes were gathered or cemented together to form larger clots. At the same depth (0 cm or 15 cm), the soil skeleton particle size was uniform and densely arranged after reinforcement by the PAVP test, while the soil skeleton particle size was disordered and loosely arranged after reinforcement by the TAVP test.

4.2.1.2 Skeleton particle contact forms

Both forms of contact (point contact and surface contact) were observed in the soil microstructure of the two methods at different depths. After the PAVP treatment, the contact forms of the soil skeleton particles were mostly surface contacts, with only a small number of point contacts; after the TAVP treatment, the contact forms of the soil skeleton particles were more evenly split between point contacts and surface contacts.

4.2.1.3 Intraframework grain pores

At identical depths, the diameters of the pores between the soil skeletons in the TAVP method were large, and there were a large number of intergranular pores. However, the diameters of the pores between the soil skeletons in the PAVP method were small; the pores were mainly intragranular pores, and the intergranular pores were small. The strongest effect on soil deformation was the number of intergranular pores, followed by that of the intragranular pores, while the effect of the interparticle pores was smaller, and that of intracavity pores was negligible (Delage and Lefebvre, 1984; Zhang et al., 2018a, 2018b). These findings indicated that compared with the TAVP test, the microstructure of the PAVP test was not prone to deformation, and its consolidation behavior was better.

In summary, the above mentioned results showed that the consolidation behavior of Tianjin
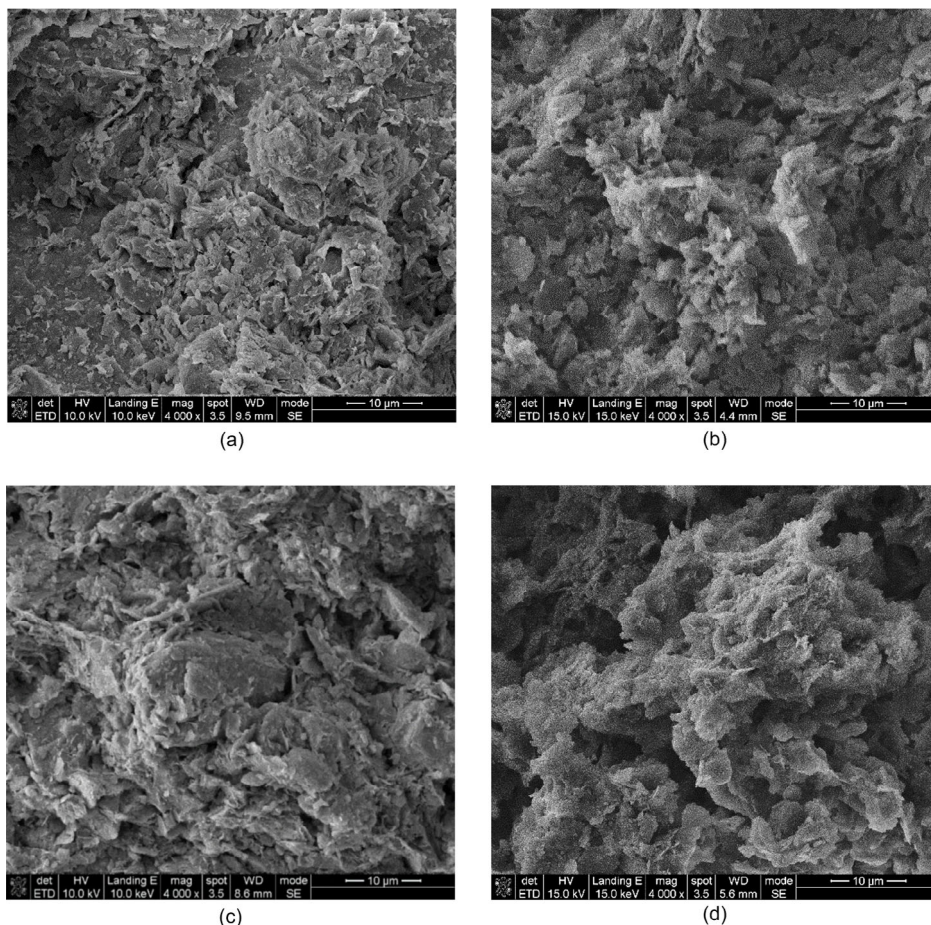

Fig. 12 SEM images of measuring point S3 after reinforcement: (a) 0 cm depth, PAVP test; (b) 0 cm depth, TAVP test; (c) 15 cm depth, PAVP test; (d) 15 cm depth, TAVP test

dredged clay using the PAVP method was superior to that from the TAVP method with regard to the three aspects: skeleton particle morphologies, skeleton particle contact forms, and intraframework grain pores.

4.2.2 Quantitative analysis of the microstructures

Quantitative analysis of the microstructures of dredged clay was carried out. It can be divided into two aspects: porosity and fractal dimension (D). Table 6 provides the quantitative parameters of the microstructure derived from SEM images; the results were obtained by binarizing the images. The specific analysis results were as follows:

Table 6 Quantitative parameters of the microstructure observed in the SEM images

Method	Measuring point	Depth (cm)	Porosity (%)	Fractal dimension, D
PAVP	S1	0	4.2	1.008
	S2	0	7.5	1.123
	S3	0	9.5	1.155
TAVP	S1	0	6.8	1.176
	S2	0	12.0	1.183
	S3	0	7.5	1.201
PAVP	S1	15	4.9	1.177
	S2	15	8.8	1.159
	S3	15	6.3	1.142
TAVP	S1	15	7.6	1.226
	S2	15	13.3	1.199
	S3	15	8.2	1.216

4.2.2.1 Porosity

At similar depths (0 cm or 15 cm) of the three measuring points, except S3 at depth 0 cm, the porosity in the soil after PAVP reinforcement was low, while that after TAVP reinforcement was high. For instance, at a depth of 0 cm, the maximum values of the porosity were 9.5% and 12.0% for the PAVP and TAVP methods, respectively. These results demonstrated that compared with the TAVP method, the PAVP method could cause a decrease in the porosity of approximately 20.8%. This was because the pore diameter and connectivity between the soil skeletons after the PAVP reinforcement were lower than those after the TAVP reinforcement. In addition, at different depths, the porosity at depth 0 cm was lower than that at depth 15 cm, except for S3 of PAVP. These results

corresponded to the model test results of the shallow (0 cm) reinforcement effect being better than the deep (15 cm) reinforcement effect.

4.2.2.2 Fractal dimension

The D values of the soil pores after PAVP reinforcement were lower than those of the soil pores after TAVP reinforcement at equivalent depths (0 cm or 15 cm) of the three measuring points. The maximum values for the PAVP and TAVP methods were 1.177 and 1.226, respectively. This was because when the soil had been reinforced by vacuum preloading, the pores due to the PAVP method were small and uniform, and the degree of irregularity was low, while the pores due to the TAVP method were large and disordered, and the degree of irregularity was high. Consequently, the soil in the PAVP method had to be subjected to a larger force to destroy the existing equilibrium state, which explained why the strength of the soil after PAVP reinforcement in the model test was higher than that of the soil after TAVP reinforcement.

According to the above findings, one could deduce that the consolidation behavior of Tianjin dredged clay by the PAVP method had clear advantages over that of the TAVP method in respect of the two quantitative parameters of porosity and fractal dimension.

4.2.3 Pore diameter distributions

The microstructures of the clay at the different measuring points (M1, M2, and M3) and depths (0 cm and 15 cm) after reinforcement were explored by MIP. The pore diameter distributions of the dredged clay after PAVP and TAVP reinforcements are shown in Fig. 13. It can be seen that at the different depths and three measuring points, the overall change trend of the volume proportion with the pore diameter was similar; in both methods, the peak position of the PAVP reinforcement was observed on the left side of that of the TAVP reinforcement, indicating that there were more small pores in the PAVP test.

Since the behaviors of the pore diameter distribution at the three measuring points were parallel, the pore diameter distributions of the soil samples strengthened by the two methods were analyzed only at measuring point M1 (Fig. 13a).

At a depth of 0 cm at measuring point M1, both curves showed a distinct peak, but the positions and

magnitudes of the peaks were different. For the soil sample strengthened by the PAVP method, the peak value of the curve was observed near a pore diameter of 0.10 μm, and the peak value of the volume proportion was approximately 6.4%. However, for the soil sample after TAVP reinforcement, the pore diameter for the peak value was approximately 1.05 μm, and the peak value of the volume proportion was approximately 4.0%. These results indicated that the small-diameter pores were the dominant pore

(a)

(b)

(c)

Fig. 13 Pore diameter distributions of the dredged clay after reinforcement at measuring points M1 (a), M2 (b), and M3 (c)

groups after reinforcement by the PAVP method, and the large-diameter pores were the dominant pore groups after reinforcement by the TAVP method, which was completely consistent with the results observed in the SEM images. Thus, the consolidation behavior of the clay using the PAVP method was superior to that of the TAVP method.

At a depth of 15 cm at measuring point M1, the overall behavior was consistent with that at a depth of 0 cm, but the peak positions of the two reinforcement modes had shifted to the right. For the soil sample, the PAVP method resulted in a peak curve near a pore diameter of 0.26 μm, and the peak value of the volume proportion was approximately 2.8%. For the soil sample from the TAVP method, the pore diameter for the peak value was approximately 5.58 μm, and the peak value of the volume proportion was approximately 2.9%. These findings indicated that in both reinforcement modes, the number of large-diameter pores in the soil increased with increasing depth.
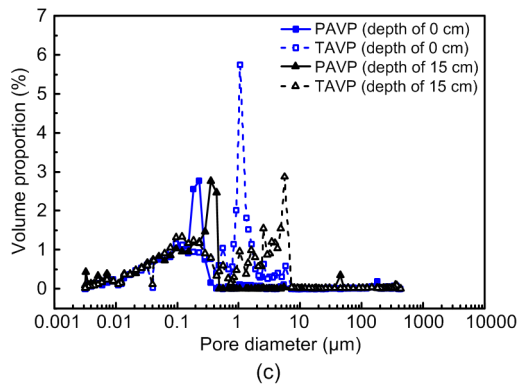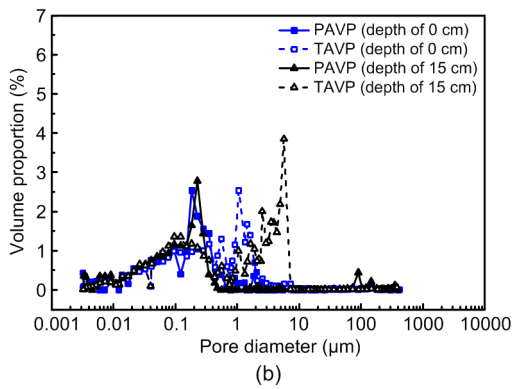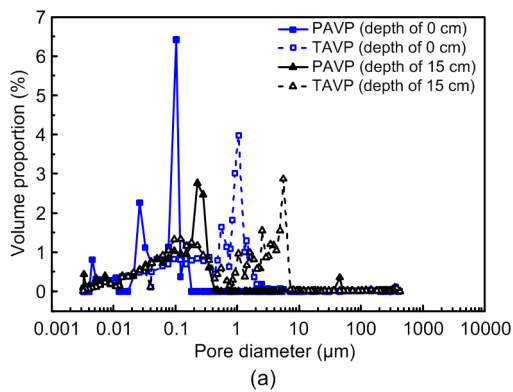
5 Discussion

The pressure difference between water-draining PVDs and the air-booster PVD/tube AVP method is one of the main reasons for promoting drainage and accelerating consolidation (Shen et al., 2015; Lei et al., 2017a, 2020; Cai et al., 2018). The action directions of air-booster pressure in the two methods are presented in Fig. 14. In the PAVP method (Fig. 14a), the direction of air-booster pressure acts only in two opposite directions, and the action direction is perpendicular to the water-draining PVDs, whereas in the TAVP method (Fig. 14b), the direction of air-booster pressure acts in multiple directions, and only part of the pressure is perpendicular to the water-draining PVDs. However, the air-booster pressure perpendicular to the water-draining PVDs has the greatest effect on increasing the pressure difference between water-draining PVDs and air-booster PVD; therefore, compared with TAVP, PAVP can further reinforce Tianjin dredged clay in these experiments.

6 Conclusions

In this study, the consolidation behaviors of Tianjin dredged clay using the PAVP and TAVP
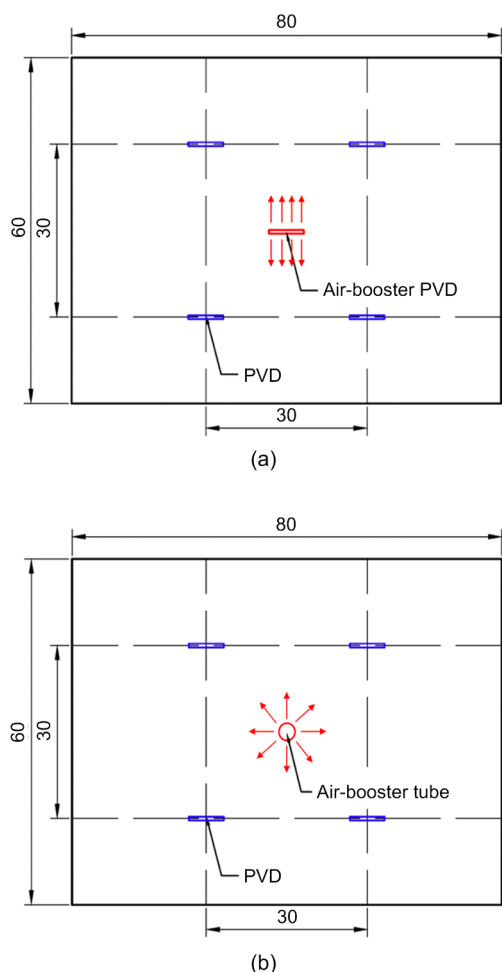
(a)

(b)

Fig. 14   Action directions of air-booster pressure: (a) PAVP; (b) TAVP (unit: cm)

methods were investigated by both model and microstructure tests. Among them, the two sets of model test were compared to evaluate the consolidation behavior of the clay by the PAVP and TAVP methods from a macroscopic point of view, and microstructure tests of the clay after reinforcement by the two methods were performed to analyze the changes in the microstructure. Based on the results of the model and microstructure tests, the conclusions can be summarized as follows:

1. The model test results showed that the consolidation behavior of Tianjin dredged clay using the PAVP method is better than that using the TAVP method from a macro point of view. The specific performance was as follows: (1) The water discharge, consolidation settlement, and dissipation of the pore-water pressure of the PAVP test were 13.85%, 14.39%,

and 12.40% greater than those of the TAVP test, respectively. (2) The PAVP test could clearly decrease the water content by 19.34% and significantly increase the dry density, vane shear strength, foundation bearing capacity, and DOC.

2. The microstructure test results indicated that the consolidation behavior of Tianjin dredged clay using the PAVP method had clear advantages over that of the TAVP method from a micro perspective. The specific results could be divided according to the following aspects: (1) In the SEM test, compared with the results of the TAVP method, after PAVP reinforcement the skeleton particle morphology was more uniform and denser, the contact forms of the particles consisted more of surface contacts, and the intraframework grain porosity was higher; in addition, the porosity and fractal dimension of the soil were smaller. (2) In the MIP test, the peak position of the pore diameter distribution for the PAVP test was observed on the left side of that for the TAVP test, indicating that there were smaller pores in the PAVP test.

3. In summary, the consolidation behavior of Tianjin dredged clay using the PAVP method was better than that using the TAVP method based on the model and microstructure tests, which could more efficiently relieve water-draining PVD clogging and significantly accelerate drainage consolidation.

Contributors

Hua-yang LEI, Yao HU, and Jing-jin LIU designed the research. Yao HU and Chen-yuan LI processed the corresponding data. Yao HU wrote the first draft of the manuscript. Hua-yang LEI, Jing-jin LIU, and Xu LIU helped to organize the manuscript. Hua-yang LEI and Yao HU revised and edited the final version.

Conflict of interest

Hua-yang LEI, Yao HU, Jing-jin LIU, Xu LIU, and Chen-yuan LI declare that they have no conflict of interest.

References

Arasan S, Akbulut S, Hasiloglu AS, 2011. The relationship between the fractal dimension and shape properties of particles. *KSCE Journal of Civil Engineering*, 15(7): 1219-1225.
https://doi.org/10.1007/s12205-011-1310-x

Azari B, Fatahi B, Khabbaz H, 2016. Assessment of the elastic-viscoplastic behavior of soft soils improved with vertical drains capturing reduced shear strength of a

disturbed zone. *International Journal of Geomechanics*, 16(1):B4014001.
https://doi.org/10.1061/(ASCE)GM.1943-5622.0000448

Bergado DT, Balasubramaniam AS, Fannin RJ, et al., 2002. Prefabricated vertical drains (PVDs) in soft Bangkok clay: a case study of the new Bangkok International Airport project. *Canadian Geotechnical Journal*, 39(2):304-315.
https://doi.org/10.1139/t01-100

Cai YQ, Qiao HH, Wang J, et al., 2017. Experimental tests on effect of deformed prefabricated vertical drains in dredged soil on consolidation via vacuum preloading. *Engineering Geology*, 222:10-19.
https://doi.org/10.1016/j.enggeo.2017.03.020

Cai YQ, Xie ZW, Wang J, et al., 2018. New approach of vacuum preloading with booster prefabricated vertical drains (PVDs) to improve deep marine clay strata. *Canadian Geotechnical Journal*, 55(10):1359-1371.
https://doi.org/10.1139/cgj-2017-0412

Chai JC, Miura N, Nomura T, 2004. Effect of hydraulic radius on long-term drainage capacity of geosynthetics drains. *Geotextiles and Geomembranes*, 22(1-2):3-16.
https://doi.org/10.1016/S0266-1144(03)00048-7

Chai JC, Hayashi S, Carter JP, 2006. Vacuum consolidation and its combination with embankment loading. Geo-Shanghai International Conference, p.177-184.
https://doi.org/10.1061/40864(196)24

Chu J, Yan SW, 2015. Application of the vacuum preloading method in soil improvement projects. *Elsevier Geo-Engineering Book Series*, 3:91-117.
https://doi.org/10.1016/S1571-9960(05)80006-0

Chu J, Yan SW, Yang H, 2000. Soil improvement by the vacuum preloading method for an oil storage station. *Géotechnique*, 50(6):625-632.
https://doi.org/10.1680/geot.2000.50.6.625

Delage P, Lefebvre G, 1984. Study of the structure of a sensitive Champlain clay and of its evolution during consolidation. *Canadian Geotechnical Journal*, 21(1):21-35.
https://doi.org/10.1139/t84-003

Hyslip JP, Vallejo LE, 1997. Fractal analysis of the roughness and size distribution of granular materials. *Engineering Geology*, 48(3-4):231-244.
https://doi.org/10.1016/S0013-7952(97)00046-X

Indraratna B, Sathananthan I, Rujikiatkamjorn C, et al., 2005. Analytical and numerical modeling of soft soil stabilized by prefabricated vertical drains incorporating vacuum preloading. *International Journal of Geomechanics*, 5(2): 114-124.
https://doi.org/10.1061/(ASCE)1532-3641(2005)5:2(114)

Indraratna B, Rujikiatkamjorn C, Balasubramaniam AS, 2014. Consolidation of estuarine marine clays for coastal reclamation using vacuum and surcharge loading. Geo-Congress, p.358-369.
https://doi.org/10.1061/9780784413265.029

Inyang HI, Bae S, Mbamalu G, et al., 2007. Aqueous polymer effects on volumetric swelling of Na-montmorillonite.

Journal of Materials in Civil Engineering, 19(1):84-90.
https://doi.org/10.1061/(ASCE)0899-1561(2007)19:1(84)

Katsman R, Ostrovsky I, Makovsky Y, 2013. Methane bubble growth in fine-grained muddy aquatic sediment: insight from modeling. *Earth and Planetary Science Letters*, 377-378:336-346.
https://doi.org/10.1016/j.epsl.2013.07.011

Lei HY, Qi ZY, Zhang ZP, et al., 2017a. New vacuum-preloading technique for ultrasoft-soil foundations using model tests. *International Journal of Geomechanics*, 17(9):04017049.
https://doi.org/10.1061/(ASCE)GM.1943-5622.0000934

Lei HY, Li X, Wang L, et al., 2017b. Reinforcement effect of polyacrylamide on dredger fill improved by vacuum preloading. Proceedings of the International Conference on Transportation Infrastructure and Materials.
https://doi.org/10.12783/dtmse/ictim2017/10077

Lei HY, Hu Y, Zheng G, et al., 2020. Improved air-booster vacuum preloading method for newly dredged fills: laboratory model study. *Marine Georesources & Geotechnology*, 38(4):493-510.
https://doi.org/10.1080/1064119X.2019.1599088

Li LH, Wang Q, Wang NX, et al., 2009. Vacuum dewatering and horizontal drainage blankets: a method for layered soil reclamation. *Bulletin of Engineering Geology and the Environment*, 68(2):277-285.
https://doi.org/10.1007/s10064-009-0200-7

Liu JJ, Lei HY, Zheng G, et al., 2017. Laboratory model study of newly deposited dredger fills using improved multiple-vacuum preloading technique. *Journal of Rock Mechanics and Geotechnical Engineering*, 9(5):924-935.
https://doi.org/10.1016/j.jrmge.2017.03.003

Liu JJ, Lei HY, Zheng G, et al., 2018. Improved synchronous and alternate vacuum preloading method for newly dredged fills: laboratory model study. *International Journal of Geomechanics*, 18(8):04018086.
https://doi.org/10.1061/(ASCE)GM.1943-5622.0001220

Ong CY, Chai JC, 2011. Lateral displacement of soft ground under vacuum pressure and surcharge load. *Frontiers of Architecture and Civil Engineering in China*, 5(2):239.
https://doi.org/10.1007/s11709-011-0110-1

Shen YP, Wang HH, Tian YH, et al., 2015. A new approach to improve soft ground in a railway station applying air-boosted vacuum preloading. *Geotechnical Testing Journal*, 38(4):373-386.
https://doi.org/10.1520/GTJ20140106

Wang J, Cai YQ, Ma JJ, et al., 2016. Improved vacuum preloading method for consolidation of dredged clay-slurry fill. *Journal of Geotechnical and Geoenvironmental Engineering*, 142(11):06016012.
https://doi.org/10.1061/(ASCE)GT.1943-5606.0001516

Wang J, Ni JF, Cai YQ, et al., 2017. Combination of vacuum preloading and lime treatment for improvement of dredged fill. *Engineering Geology*, 227:149-158.
https://doi.org/10.1016/j.enggeo.2017.02.013

Wang J, Zhao R, Cai YQ, et al., 2018. Vacuum preloading and electro-osmosis consolidation of dredged slurry pre-treated with flocculants. *Engineering Geology*, 246:123-130.
https://doi.org/10.1016/j.enggeo.2018.09.024

Wang J, Huang G, Fu HT, et al., 2019. Vacuum preloading combined with multiple-flocculant treatment for dredged fill improvement. *Engineering Geology*, 259:105194.
https://doi.org/10.1016/j.enggeo.2019.105194

Yan SW, Chu J, 2005. Soil improvement for a storage yard using the combined vacuum and fill preloading method. *Canadian Geotechnical Journal*, 42(4):1094-1104.
https://doi.org/10.1139/t05-042

Ye T, 2018. Experimental Observation and Theoretical Analysis on the Bubbles' Shape within Transparent Soft Soil. MS Thesis, Zhejiang University, Hangzhou, China (in Chinese).

Yu C, Wang H, Zhou AN, et al., 2019. Experimental study on strength and microstructure of cemented soil with different suctions. *Journal of Materials in Civil Engineering*, 31(6):04019082.
https://doi.org/10.1061/(asce)mt.1943-5533.0002717

Zhang T, Cai GJ, Liu SY, 2018a. Application of lignin-stabilized silty soil in highway subgrade: a macroscale laboratory study. *Journal of Materials in Civil Engineering*, 30(4):04018034.
https://doi.org/10.1061/(ASCE)MT.1943-5533.0002203

Zhang T, Cai GJ, Liu SY, 2018b. Reclaimed lignin-stabilized silty soil: undrained shear strength, Atterberg limits, and microstructure characteristics. *Journal of Materials in Civil Engineering*, 30(11):04018277.
https://doi.org/10.1061/(ASCE)MT.1943-5533.0002492

Zheng G, Liu JJ, Lei HY, et al., 2017. Improvement of very soft ground by a high-efficiency vacuum preloading method: a case study. *Marine Georesources & Geotechnology*, 35(5):631-642.
https://doi.org/10.1080/1064119X.2016.1215363